Physica A 195 (1993) 12–30
North-Holland

PHYSICA A

Phase transitions in a monolayer of interconverting squares

Diego Kramer and Avinoam Ben-Shaul

Department of Physical Chemistry and The Fritz Haber Research Center for Molecular Dynamics, The Hebrew University, Jerusalem 91904, Israel

Received 9 October 1992
Revised manuscript received 17 November 1992

The two successive fluid–fluid phase transitions in surfactant Langmuir monolayers are described using a highly simplified molecular model: a 'reactive' mixture of inter-converting squares of two different sizes. The model is solved by a mean-field lattice approach and by Monte Carlo simulations. The mean-field scheme involves a re-division of the original lattice into 'cells' which can contain either one large square representing the (projection on the lattice of) an amphiphilic molecule in a conformationally disordered ('expanded') state, or clusters consisting of 1–4 small squares, each representing an ordered ('stretched') molecule. This procedure circumvents some of the difficulties associated with the size disparity of the adsorbed particles. In spite of its simplicity, the model can explain some major, as well as some subtle, characteristics of experimental monolayer phase diagrams. These include the conditions under which the monolayer exhibits one phase transition, two or none; the decrease of the triple point temperature with increasing chain length, and the gradual decrease with temperature of the liquid-condensed phase density.

1. Introduction

Upon compression of a Langmuir monolayer, the amphiphilic molecules adsorbed at the air–water interface undergo changes in both their state of aggregation and their internal structure. This coupling between the external (translational) and internal (conformational and/or orientational) degrees of freedom of the adsorbed molecules is responsible for the rich phase behavior of Langmuir monolayers [1,2]. At very high surface densities (coverages) the amphiphilic chains must fully stretch out in order to allow for efficient packing, thus sacrificing conformational freedom. In this regime a variety of crystalline phases, corresponding to different combinations of positional and orientational order (or tilt-angle) of the (stretched) chains have been observed in experiments and computer simulations [3]. At lower coverages the chains are flexible

and the monolayer is a two-dimensional (2D) fluid. A most remarkable common characteristic of this regime is the appearance of *two* successive first order fluid–fluid phase transitions [2,4–11]: A transition from a 2D gas phase to a 'liquid-expanded' phase (a g–le transition) at low densities, followed upon further compression, by a le–lc transition from the expanded to a 'liquid-condensed' phase. In monolayers of pentadecanoic acid, for example, the areas per molecule in the coexisting phases (at room temperature) are: $a \simeq 1300$ Å^2 and 43.5 Å^2 for the g–le [4a] transition and $a \simeq 31$ Å^2 and 21.5 Å^2 for the le–lc transition [4b].

A number of theoretical studies have recently been concerned with the molecular aspects of the above phases and the 'order parameters' governing the transitions between them [8–15]. These studies include mean-field theories applied to flexible model chains, as well as Monte Carlo (MC) and mean-field analyses of monolayers of mobile rod-like particles with orientation-dependent adsorption energies (see ref. [11] for a more detailed discussion). Although the origin of the monolayer's phase behavior is somewhat differently interpreted in each model, they are all consistent with the following qualitative scheme [14]. The monolayer's free energy can be regarded as a sum of three terms $F = F_{\text{int}} + F_{\text{trans}} + F_{\text{att}}$. The first term is a sum of single-particle contributions, $F_{\text{int}} = Nf_{\text{int}}$, accounting for the internal free energy of the molecules. In the case of flexible chains, f_{int} involves the chain conformational free energy and the adsorption energy of chain segments onto the air–water interface. In the case of rod monolayers, f_{int} includes the orientational entropy of the rods and, again, the adsorption energy of rods lying on the surface. Note that, in both cases, strong adsorption implies preference of the chains (rods) to lie on the surface, thus occupying larger area fractions. $S_{\text{trans}} = -F_{\text{trans}}/T$ is the translational entropy of the monolayer, including the effects of excluded area interactions. Finally, $F_{\text{attr}} = E_{\text{attr}}$ is the free energy associated with intermolecular attractions.

At low coverages, when intermolecular interactions are negligible, the adsorbed molecules are essentially independent of each other and $f_{\text{int}} \approx f^0_{\text{int}}$ is minimal, corresponding to the free energy of an isolated chain (rod). The unperturbed ('free') chains are typically characterized by a large average cross-sectional area, owing to their large conformational freedom and/or adsorption at the interface. As the coverage increases the chains are no longer 'free', and f_{int} increases due to constraints imposed by intermolecular (primarily excluded-volume) interactions. In general, upon compression of the monolayer, the chains tend to desorb from the surface and stretch (similarly, rods stand up) in order to reduce intermolecular repulsions. Suppose, however, that $f_{\text{int}} = f^0_{\text{int}}$ were independent of coverage, then, as the coverage increases, the interplay between the increasing F_{trans} and the decreasing F_{att} will result (below

a critical temperature) in a gas–liquid condensation of the unperturbed chains. This is a possible scenario, provided F_{int} – the free energy content of the unperturbed molecule (as measured, say, with respect to a fully stretched chain state, or perpendicular rod state) – is much larger than $\Delta F_{trans} = F^{l}_{trans} - F^{g}_{trans}$ and $\Delta F_{att} = F^{l}_{att} - F^{g}_{att}$, the changes in translational and attraction free energies in the transition. Alternatively, one can say that in this g–le transition the chains need not sacrifice much conformational freedom in the liquid phase (in analogy to polymer melts). The liquid phase in this picture is an 'expanded' one, because the area per chain is comparable to the cross-sectional (or some 'effective') area of the unperturbed chains. As the density increases further, the chains must extend in order to allow for efficient packing, thus losing their conformational freedom (f_{int} increases). A second, le–lc-type first order phase transition may then take place if the loss of internal free energy can be effectively balanced by a gain in the interaction free energy, primarily F_{att}. In order that the transition will be first order, the attraction energy in the lc phase must be larger than in the le phase, otherwise the transition (loss of internal free energy) will be continuous. (In fact, it has been shown [11,12] that for a monolayer of rod-like particles no phase transition takes place without attractive interactions, as opposed to the case of a 3D system of *hard* rods where excluded volume repulsions suffice to induce an isotropic–nematic transition [16,17]). Thus, according to the above picture, two successive first order transitions are possible, provided a gas–liquid transition of nearly unperturbed molecules can be completed before strong repulsive interactions between these molecules set in. This, g–le, transition is governed by the balance between F_{trans} and F_{att} and involves a large density change. The second, le–lc, transition takes place at higher densities and is governed, primarily, by a trade-off between F_{int} and F_{att}.

If the internal free energy content of the unperturbed molecules, f^{0}_{int}, is small, as in the case of stiff or short chains and/or small adsorption energy, the intermediate, le, phase loses its special stability and the monolayer can go directly from the gas to the liquid-condensed phase. Recently this behavior has been observed experimentally, in a monolayer of stiff (perfluorinated) chains [5]. The le phase reappears when parts of the chains become flexible again by replacing the fluorine atoms by hydrogens.

In the 'direct' g→lc transition all the contributions to F change significantly and simultaneously, i.e. all degrees of freedom are strongly coupled. Other situations where only one transition, or no first order transition, is observed are also possible. Many of these cases have been demonstrated for a simple model system, namely, a monolayer of rod-like particles with three restricted orientations [11]. However, even in this simple system, complications arise, both in MC simulations and in mean-field analyses, owing to the possibility of in-plane

ordering and phase transitions of the adsorbed rods [15]. These transitions are coupled to the g–le and le–lc ('standing up') transitions in this system, which are more relevant to the behavior of surfactant monolayers. Furthermore, while rod-like particles provide a reasonable model for the stiff chains in the lc and crystalline phases, they do not appropriately represent the flexible chains in the le or g phases. In fact, in these phases an isotropic shape provides a more adequate model for the average geometry of flexible chains.

In a previous study [11] we have considered an alternative, simple, two-state model for the monolayer. The two states of the adsorbed particles mimic different groups of molecular conformations. They differ in their projected cross-sectional area on the surface, their interactions and their adsorption energies. For instance, on a 2D square lattice, a particle in state 's' ('s' = 'surface' or 'short') occupies 4 sites, whereas a particle in state 't' ('tall') occupies only one site. The s and t-particles represent 'free' (or 'expanded') and 'stretched' molecules, respectively. The two forms interconvert, i.e. their proportions at any density and temperature are determined by the conditions for 'chemical equilibrium' $s \rightleftharpoons t$. The composition of the monolayer and its state of aggregation are strongly coupled to each other, and depend sensitively on the molecular parameters specifying the internal free energy, intermolecular attractions and particle size and shape. Preliminary MC calculations on this model, corresponding to a 2D mixture of inter-converting large (s) and small (t) squares, have indicated the possibility of observing two (or less) successive monolayer phase transitions [11].

In this paper we present both MC and mean-field calculations for a similar monolayer model. The mean-field calculations are based on a variation of the Bragg–Williams approximation. More explicitly, the (square) lattice is partitioned into square, four-site, cells, such that each cell can be occupied by either one s-particle or by an i-mer ($i = 1, \ldots, 4$), i.e. a cluster of four particles. (Other lattices and other partitionings of the sites into cells may be used). The number of sites in a cell corresponds to the ratio between the projected areas of the t (stretched) and s (disordered) forms, respectively. The re-partitioning of the lattice enables the use of a single, simple, free energy for all surface densities. Using this approximation it will be shown that the mean-field treatment reproduces the same qualitative features observed in the MC simulations, including the various sequences of phase transitions.

Several other studies have employed two (or few)-state models to study monolayer or bilayer properties, e.g., a system of interconverting disks [18] has been used to study the liquid–solid transition in monolayers. Our interest, as stressed above, is to understand and demonstrate using the simplest possible model the various sequences of fluid–fluid transitions observed in Langmuir monolayers.

2. Model

We treat the surface as a square lattice comprising $\bar{M}$ *sites* of area 1×1. A t-particle occupies a single site whereas an s-particle occupies a square block of 4 sites. For the sake of concreteness one can assume, for instance, that the adsorbed particles are rectangular parallelepipeds of dimensions $1 \times 1 \times 4$ (t) and $2 \times 2 \times 1$ (s), so that their volumes are equal but their projected areas on the surface are different: 1×1 and 2×2, respectively; see fig. 1. In the mean-field model presented in the next section, we re-divide the lattice into $M = \bar{M}/4$ square 'cells' of 2×2 sites. In this model, a cell can accommodate either $i = 1, \ldots, 4$ t-particles (an 'i-cluster') or *exactly* one s-particle. This restriction on the s-particles, which is not imposed in the MC simulations, can be accounted for by a degeneracy correction factor in the partition function, as discussed in section 3.

Excluded area interactions between the adsorbed particles are taken into account by the requirement for single occupancy of lattice sites. We also include attractive interactions between nearest-neighbor (nn) particles: u_{st}, u_{tt} and u_{ss}, with u_{ss} denoting the attractive potential between two neighboring s-particles, etc. In all the numerical calculations the u's were parameterized according to the relationship

$$u_{tt} = 2u_{ss} = 4u_{st} = -4u \,, \tag{1}$$

with $u\,(u > 0)$ denoting the energy of attraction, per unit 'contact area', between two nn particles. For instance, the contact area between two t-particles (of dimensions $1 \times 1 \times 4$) occupying nn sites is 4, etc.

We use f_s to denote the internal ('self') free energy of an isolated s-particle,

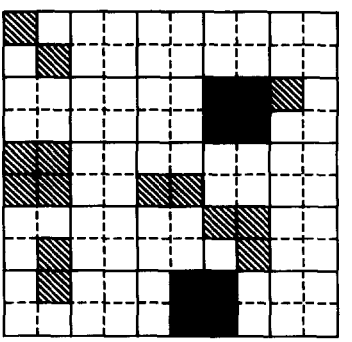

Fig. 1. Schematic two-dimensional representation of the lattice model. The solid lines divide the lattice into cells, each containing four sites (broken lines). Large (solid black) and small (hatched) squares represent the projections of the s and t-particles, respectively.

and similarly, f_t for the t-particle. $z_s = \exp(-\beta f_s)$ and $z_t = \exp(-\beta f_t)$ are the corresponding internal partition functions, $\beta = 1/kT$. f_s and f_t represent the sum of the adsorption energy and the conformational degeneracy of the 'expanded' and 'condensed' ('stretched') forms of the adsorbed molecules, respectively. As argued in the previous section, we expect $\Delta f = f_s - f_t < 0$. Δf, or equivalently, the 'equilibrium constant'

$$\kappa = \frac{z_s}{z_t} = \exp(-\beta\,\Delta f) = \left(\frac{X_s^*}{X_t^*}\right)_{\rho\to 0}, \tag{2}$$

determines the relative proportions of t and s-particles in the limit of zero monolayer coverage, i.e. in the absence of inter-particle interactions. We use $X_s = N_s/N$ and $X_t = 1 - X_s$ to denote a given monolayer composition, N_s and N_t being the number of molecules of each species, $N_s + N_t = N$ is the total number of particles. $X_s^* = N_s^*/N = 1 - X_t^*$ is the equilibrium (most probable) composition, $\rho = N/\bar{M} = N/4M$ is the total 2D number density. Note that the maximal density $\rho_{max} = N_{t,max}/\bar{M} = 1$ corresponds to a surface which is fully covered by t-particles ($N = N_t$). On the other hand, when the surface is fully covered by s-particles, $\rho = N_{s,max}/\bar{M} = 0.25$. In general $0 \leq \rho \leq 1$.

3. Mean-field theory

The division of the surface into $M = \bar{M}/4$ 4-site cells enables us to treat the monolayer as a reactive lattice-gas mixture of 5 species: s-particles and $i = 1, \ldots, 4$ clusters distributed over the M cells. (Equivalently, the monolayer can be treated as a 6-species mixture if we consider a vacant cell as an additional occupation state, which could be treated as an $i = 0$ cluster). Note that the s-squares are not allowed to overlap (i.e. occupy sites belonging to) different cells. This implies that each of the 6 species occupies the same (one cell) area. The equilibrium composition of the mixture, $N_s^*, \{N_i^*\}$, will be determined, later on, by minimization of the system's free energy. N_i denotes the number of lattice cells which, at a given surface configuration, contain i small squares and N_s is the number of cells occupied by s-squares. The N_i satisfy the particle conservation condition $\Sigma\, iN_i = N_t$. We also use $\rho_i = N_i/M$, $\rho_s = N_s/M$ and $\rho_0 = N_0/M$ to denote the fractions of cells occupied by i-clusters, s-squares and empty cells, respectively. The ρ_i satisfy the conservation condition $\Sigma\, i\rho_i = N_t/M$. Note the equalities $\rho_s + \Sigma\rho_i + \rho_0 = 1$ and $\rho_s + \Sigma\, i\rho_i = 4\rho$.

To calculate the thermodynamic properties of the system we need to define cell internal partition functions, and cell–cell interaction energies. These quantities can be expressed in terms of the z_k's and u_{kl}'s introduced in the

previous section. To this end we note that any monolayer configuration $\Phi(N_s, N_t)$, corresponding to a given distribution of the N_s and N_t particles on the $\bar{M}$ sites of the surface, can be characterized by the states $\phi_1, \ldots, \phi_M$ of the different cells. The possible states are: $\phi = 0$, denoting a vacant cell; $\phi = s$ denoting a cell occupied by an s-particle, and $\phi = i_p$ denoting a cell containing i t-particles arranged in configuration p among the 4 sites. (There are $4!/i!(4-i)!$ states for a cell containing i t-particles).

The internal partition function of an i-cluster is given by

$$q_i = z_t^i \sum_p \exp(-\beta n_{ip} u_{tt}) , \tag{3}$$

with n_{ip} denoting the number of nn contacts between the t-particles. For the s-particle we take $q_s = 4z_s$. The additional 'degeneracy' factor of 4 is introduced in order to compensate for the loss of configurational entropy by the s-particles due to their restriction to only $M/\bar{M} = 1/4$ of the sites of the original lattice; a restriction which has not been imposed on the t-particles. (The reason for introducing this correction factor is to ensure that, at least in the low density limit, the results of the mean-field approximation will converge to those of the MC simulations. Alternatively, we could of course perform MC simulations with the same restriction on the s-particles as in the mean-field treatment). We also define $q_0 = 1$ as the partition function of a vacant cell.

The interaction energies, $w_{\phi\phi'}$, between two nn cells in states ϕ and ϕ' follow immediately from the definitions of the u_{kl}'s. Namely, $w_{00} = w_{0\phi} = w_{\phi 0} = 0$. $w_{ss} = u_{ss} = -2u$. $w_{s,ip} = n_{s,ip} u_{st} = -n_{s,ip} u$ and $w_{ip,jq} = n_{ip,jq} u_{tt} = -4n_{ip,jq} u$, with $n_{s,ip}$ and $n_{ip,jq}$ denoting, respectively, the numbers of s–t and t–t contacts between particles belonging to nn cells. By averaging over the cell internal states we can obtain effective interaction energies w_{si} and w_{ij} between s-particles and i-clusters, and between i and j-clusters, respectively. In deriving these potentials we ignore interactions with cells surrounding the interacting pair. Thus,

$$w_{ij} = \frac{\Sigma_{p,q} w_{ip,jq} \exp(-\beta w_{ip,jq})}{\Sigma_{p,q} \exp(-\beta w_{ip,jq})} , \tag{4}$$

with $w_{si} = w_{is}$ defined analogously.

Now the monolayer can be treated as a reactive gas mixture of 5 species: s-particles and $i = 1$–4 clusters of t-particles, occupying equal-size cells, with internal partition function q_s and q_i and with interaction energies w_{si}, w_{ij} and w_{ss} between nearest-neighbour cells. The canonical partition function of the system is

$$Q(N, M, T) = \sum_{N_s, \{N_j\}} q_s^{N_s} \prod_{i=1}^{4} q_i^{N_i} \sum_{\Phi} \exp[-\beta W(\Phi; N_s, \{N_i\})], \tag{5}$$

with $W(\Phi; N_s, \{N_i\})$ denoting the potential energy of a mixture of composition $N_s, \{N_i\}$ in configuration Φ. The first sum extends over all compositions satisfying the particle conservation condition $N_s + \Sigma_{i=1}^{4} iN_i = N$. The Φ summation includes all distinct configurations corresponding to the given composition $N_s, \{N_i\}$.

At this point we introduce the Bragg–Williams approximation [21] whereby $W(\Phi; N_s, \{N_i\})$ is replaced by its mean-field average $\tilde{W}(N_s, \{N_i\})$,

$$\tilde{W} = 2(N_s^2/M)w_{ss} + 4N_s \sum_{i=1}^{4} (N_i/M)w_{si} + 2 \sum_{i,j}^{4} (N_i N_j/M)w_{ij}, \tag{6}$$

corresponding to a random distribution of the N_s s-particles and N_i i-clusters on the surface. Now the Φ summation yields the degeneracy factor $M!/N_s!N_0!\Pi N_i!$ and (5) becomes

$$\begin{aligned} Q(N, M, T) &= \sum_{N_s, \{N_i\}} Q(N_s, \{N_i\}, M, T) \\ &= \sum_{N_s \{N_i\}} \frac{M!}{N_s!N_0!} q_s^{N_s} \prod_i \frac{q_i^{N_i}}{N_i!} \exp[-\beta \tilde{W}(N_s, \{N_i\})], \end{aligned} \tag{7}$$

with $Q(N_s, \{N_i\}, M, T)$ denoting the partition function of a mixture with fixed composition.

As usual, the system's free energy, the equilibrium composition and all other thermodynamic properties can be derived using the maximum-term method. Namely, the Helmholtz free energy $F = -kT \ln Q(N, M, T)$ is replaced by (its minimum) $F^* = F(N_s^*, \{N_i^*\}, M, T) = -kT \ln Q(N_s^*, \{N_i^*\}, M, T)$, with $Q(N_s^*, \{N_i^*\}, M, T)$ representing the maximal term in (7). $N_s^*, \{N_i^*\}$ is the most probable, i.e. the equilibrium, composition.

The equilibrium composition, $\rho_s^*, \{\rho_i^*\}$, of the system is the one which minimizes the free energy (cf. (7)),

$$\begin{aligned} F/M &= kT\rho_s \ln(\rho_s/q_s) + kT \sum_{i=1}^{4} \rho_i \ln(\rho_i/q_i) \\ &\quad + kT\rho_0 \ln \rho_0 + 2\rho_s^2 w_{ss} + 4\rho_s \sum_{i=1}^{4} \rho_i w_{si} + 2 \sum_{i,j=1}^{4} \rho_i \rho_j w_{ij}, \end{aligned} \tag{8}$$

subject to the particle conservation constraint

$$\rho_s + \sum_{i=1}^{4} i\rho_i = N/M = 4N/\bar{M} = 4\rho \,. \tag{9}$$

In (8), ρ_0 is the fraction of vacant cells

$$\rho_0 \equiv N_0/M = 1 - \rho_s - \sum_{i=1}^{4} \rho_i \,. \tag{10}$$

Before determining the equilibrium composition we derive the expressions for the pressure, π, and chemical potentials, μ_s and μ_i, for a system with composition $\rho_s, \{\rho_i\}$. From (8), using $\pi = -(\partial F/\partial M)_{T,N_s,\{N_i\}}$, we obtain

$$\pi = -kT \ln \rho_0 + 2\rho_s^2 w_{ss} + 4\rho_s \sum_{i=1}^{4} \rho_i w_{si} + 2 \sum_{i,j=1}^{4} \rho_i \rho_j w_{ij} \,, \tag{11}$$

where it should be noted that the surface area is measured in units of the cell area. Similarly, from $\mu_k = \partial F/\partial N_k$ we get

$$\mu_k = -kT \ln q_k + kT \ln(\rho_k/\rho_0) + 4\rho_s w_{sk} + 4 \sum_{j=1}^{4} \rho_j w_{kj} \,, \tag{12}$$

with $k = s$ for s-particles and $k = i$ for i-clusters.

Using the Lagrange multipliers method it is easily shown that the ρ_i's and ρ_s which minimize (8) subject to (9) are given by

$$\rho_s = \rho_0 q_s \, e^{\beta\mu} \exp\left[-\beta\left(4\rho_s w_{ss} + 4 \sum_{i=1}^{4} \rho_i w_{si}\right)\right] , \tag{13}$$

$$\rho_i = \rho_0 q_i \, e^{i\beta\mu} \exp\left[-\beta\left(4\rho_s w_{si} + 4 \sum_{j} \rho_j w_{ij}\right)\right] \qquad (i = 1\text{–}4) \,, \tag{14}$$

where it should be understood that ρ_s, ρ_i stand for their most probable (equilibrium) values ρ_s^*, ρ_i^*. Here μ is the Lagrange multiplier conjugate to the conservation constraint (9).

Comparing (13) and (14) with (12) we find, as expected, that at the equilibrium composition

$$\mu = \mu_s = \mu_i/i \qquad (\text{all } i) \,, \tag{15}$$

revealing that μ is, simply, the chemical potential of the s-particles or, equivalently, the chemical potential per t-particle ($\mu_t = \mu_i/i$) in any of the i-clusters. Of course, (15) is also the condition for chemical equilibrium in the multicomponent reactive mixture of s-particles and i-clusters; e.g., $i\mu_s = \mu_i$ is the equilibrium condition for the reaction i-cluster $\rightleftharpoons i$(s-particles), etc.

Eqs. (13) and (14) together with (9) and (10) provide seven *self-consistency* relationships between ρ_s, ρ_0, $\rho_1, \ldots, \rho_4$ and μ, from which all these quantities can be evaluated numerically for given ρ, T and given molecular parameters. Alternative representations of these equations may be convenient for numerical manipulations, or for demonstrating additional aspects of the mean-field approach. For instance, using (9) and (10), we can rewrite (13) and (14) in the form

$$\rho_s = \tilde{q}_s \lambda / \xi \,, \qquad \rho_i = \tilde{q}_i \lambda^i / \xi \,. \tag{16}$$

Here

$$\tilde{q}_k = q_k \exp\left[-\beta \left(4\rho_k w_{sk} + 4 \sum_{j=1}^{4} \rho_j w_{kj} \right) \right] \tag{17}$$

is an effective 'one-particle' partition function of an s-particle ($k = s$) or an i-cluster ($k = i$) in the mean-field of its neighbors. $\lambda = \exp(\beta\mu)$ is the absolute activity and

$$\xi = q_0 + \tilde{q}_s \lambda + \sum_{i=1}^{4} \tilde{q}_i \lambda^i \tag{18}$$

is an effective grand-canonical partition function of one cell. $q_0 = 1$, $\tilde{q}_s$ and the $\tilde{q}_i$ correspond to the different possible occupations of the cell. According to this representation, ρ_s in (16) is the probability of finding the cell occupied by an s-particle, etc. The conservation constraint (9) is now represented by $\rho_s + \Sigma\, i\rho_i = \partial \ln \xi / \partial \ln \lambda$.

Numerical solutions of the self-consistency equations (13), (14) (equivalently (16)) for different choices of monolayer parameters and thermodynamic conditions are presented in the next section. We shall see that the simple model described in this section can provide an explanation for the conditions under which the monolayer exhibit one, two or no phase transitions, and account for the monolayer composition in the different phases.

4. Results and discussion

In this section we present the results of MC simulations and of the mean-field scheme described in the previous section, for the monolayer of interconverting s–t-particles. The MC simulations have been performed in the canonical (NMT) ensemble using the standard Metropolis procedure [19]. In

these simulations the particles can translate on all lattice *sites* as well as change their identity; equilibrium is ensured by the requirement for detailed balance. It should be noted that the division of the lattice into cells is not applied in the MC simulations, i.e. the s-particles are not restricted to a sub-lattice. Consequently, domain boundaries and other defects may appear in a monolayer consisting mostly of large squares, see below. (We have also performed simulations in which the s-particles are restricted to one sub-lattice, i.e. the cells. The resulting phase behavior of the monolayer is very similar in both schemes). Phase transitions in the *NMT* simulations are characterized by the appearance of large domains of the coexisting phases, and confirmed by the constant values of the $\mu(T)$ vs. $\rho = N/\bar{M} = N/4M$ and $\pi(T)$ vs. ρ isotherms in the transition region. In the following we present several simulation runs corresponding to different choices of the equilibrium constant (degeneracy ratio) κ and the interaction parameter u.

In the mean-field calculations we determine the monolayer's composition $X_s = 1 - X_t = 4\rho_s/\rho$ and chemical potential $\mu = kT \ln \lambda$ as a function of temperature T and density ρ, by solving (16) for ρ_s and $\{\rho_i\}$. From the solutions we can also calculate π, F and other properties of interest. In fact, it is more convenient to treat λ (instead of ρ) as the 'independent variable' and solve (16) for the $\{\rho_i\}$, ρ_s and hence ρ and X_t as functions of $\lambda = \exp(\beta\mu)$ and T. The possibility of a phase transition is indicated by the existence of two solutions $\rho^{(1)}, X_t^{(1)}$ and $\rho^{(2)}, X_t^{(2)}$ of (16) for the same values of μ and T. More precisely, these solutions should correspond to minima of F. As is common in mean-field theories, a third solution also exists, corresponding to a maximum of F at intermediate values of the 'order parameters' ρ, X_t. The densities and compositions of the two phases at coexistence are determined, as usual, by the requirements for equal pressures and chemical potentials

$$\pi(\rho^{(1)}, X_t^{(1)}; T) = \pi(\rho^{(2)}, X_t^{(2)}; T)\,, \tag{19}$$

$$\mu(\rho^{(1)}, X_t^{(1)}; T) = \mu(\rho^{(2)}, X_t^{(2)}; T)\,. \tag{20}$$

In general, the two order parameters, ρ and X_t, are coupled to each other, in the sense that both $\Delta\rho = \rho^{(2)} - \rho^{(1)}$ and $\Delta X_t = X_t^{(2)} - X_t^{(1)}$ are non-zero. Yet, if the transition is characterized by a large density jump and only a small change in composition, we can say that it is a gas–liquid-like transition. On the other hand, if ΔX_t is large and $\Delta\rho$ is small, the transition is predominantly 'chemical'. (The isotropic–nematic transition in liquid crystals [16, 17], with the chemical composition representing the orientational distribution of molecules, belongs to this category). We shall see below that the above characterization of a phase transition as 'predominantly gas–liquid', or 'predominantly chemical',

is valid for some combinations of the molecular parameters κ, u but is inadequate for other combinations.

Consider first the case of large κ, which means a strong 'intrinsic' preference of the adsorbed particles for the expanded s-state. Thus, at low densities the monolayer contains mostly s-particles. Both excluded-area repulsions and inter-particle attractions will affect the ratio X_t/X_s as ρ increases. When $u/kT \ll 1$, cf. (1), the monolayer behaves as a 2D mixture of inter-converting hard particles. It has been shown previously, based on mean-field (Landau and generalized van der Waals) analyses and MC simulations [11], that for this system, X_t/X_s, as well as π and μ, increase monotonically with ρ, i.e., the monolayer does not exhibit any phase transition upon compression, see fig. 2. A similar qualitative behavior has been predicted for a monolayer of mobile grafted rods, and attributed to the broken symmetry of the monolayer (as compared, say, to a 3D system of hard rods where a first order isotropic–nematic transition can take place) [11,12].

The continuous increase of X_t/X_s, π and μ with ρ (for $u/kT \ll 1$) is a property of the monolayer which is independent of the value of κ. However, when κ is large, the compression of the monolayer is characterized by two distinct stages, as is clear from fig. 2 which shows the results of the mean-field calculations for $\kappa = 100$. Since the s-form is largely preferred, it prevails until the surface is nearly fully covered by these species, i.e., as long as $\rho \leq \frac{1}{4}\rho_s^{max} = 0.25$. Above this density, further addition of particles is only possible if some of

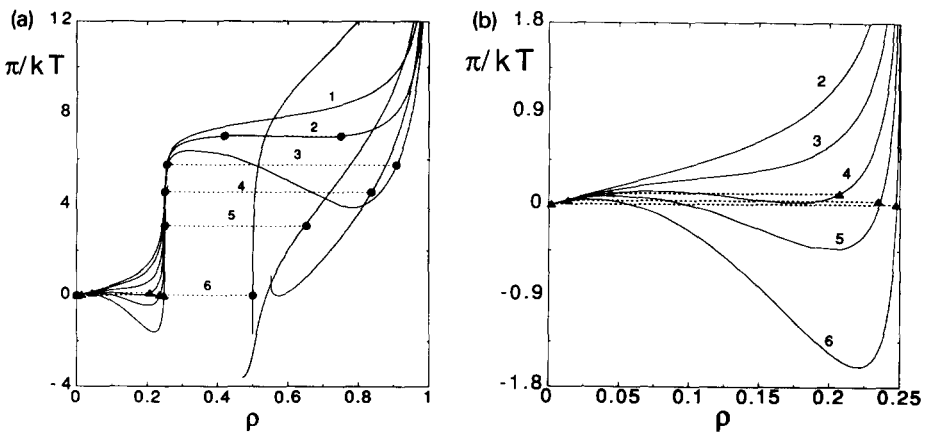

Fig. 2. (a) Pressure (π)–density (ρ) isotherms for a system with $\kappa = 100$ at $u = 0, 0.2, 0.4, 0.6, 0.8$ and $1.2kT$ (marked in increasing order). The black circles denote the densities of the coexisting c and e phases, calculated using eqs. (19), (20). The triangles denote the densities of the g and e phases. The dashed lines are tie lines. (b) Enlargement of the g–e transition region for $u = 0.2, 0.4, 0.6, 0.8$ and $1.2kT$.

the s-particles convert into their 'condensed' (stretched) t-state. The surface remains nearly fully covered, i.e. $\frac{1}{4}\sum i\rho_i + \rho_s \approx 1$, implying $X_t = 1 - X_s = 4(\rho - 1)/3\rho$, hence $X_t/X_s = (\rho - 1)/(1 - \frac{1}{4}\rho)$. MC simulations confirm this behavior.

Upon lowering T, i.e. as u/kT increases, the attractive interactions come into play and can drive either one or two first order transitions. The number and the nature of the transitions depend on κ and u/kT. From fig. 2 which shows (mean-field) $\pi-\rho$ isotherms for $\kappa = 100$, we note the following sequence. There is no first order transition at very high temperatures. Then, below some T_c^{ec}, a first order transition appears at high densities. Two transitions appear at temperatures in the range $T_{tp} < T < T_c^{ge} (< T_c^{ec})$. Then, at temperatures below T_{tp} the monolayer undergoes a single (g–c) phase transition. (We use g, e and c to denote 'gas', 'expanded' and 'condensed' states, respectively).

As T falls below a critical temperature, T_c^{ec}, corresponding to $u/kT_c^{ec} \simeq 0.2$, a first order transition appears at the high density regime ($\rho \gtrsim 0.25$). Consider for example the $u/kT = 0.4$ isotherm which shows a passage from 'low' density (yet high coverage) phase with $\rho = \rho_e \cong 0.25$ to a 'high' density (and high coverage) phase with $\rho = \rho_c \simeq 0.9$. The coexistence densities were calculated by solving (19) and (20). Not surprisingly, the solutions of (16) reveal that the lower density phase corresponds to a monolayer which is densely covered by s-particles, while the higher density phase consists mostly of t-particles. In both phases the surface is nearly fully covered by particles. The s$\rightarrow$t conversion is favored by excluded area interactions, but the transition becomes first order because of the stronger attraction between the t-particles as compared to the s-particles, see (1). More precisely, in terms of the mean-field lattice model described in section 3, it is due to the fact that at high ρ (and high u/kT) $\langle w \rangle \equiv \langle w_{ij} \rangle + w_{ss} - \langle w_{si} \rangle < 0$. ($\langle w \rangle$ increases with ρ and with u/kT because of the increasing proportions of the 'dense' $i = 4$- and 3-clusters at the expense of the dilute clusters). Since the above transition involves a large change in the chemical composition (X_t, $X_s = 1 - X_t$), i.e. in the proportions of particles in the 'expanded' and 'condensed' forms, we shall refer to it as a 'chemical', or an e–c, transition. (It is analogous to the 'standing up' transition in rod monolayers [11,12]).

We note from fig. 2 that as T falls below T_c^{ec} ($u/kT_c^{ec} \simeq 0.2$), the density gap between the coexisting phases, $\rho_c - \rho_e$, first increases (as usual) but then, around $u/kT \simeq 0.4$, it begins to narrow down. More precisely, ρ_c starts decreasing as soon as ρ_e saturates at $\rho_e = 0.25$, corresponding to full coverage of the surface by s-particles. This latter point is revealed by the calculation of the chemical composition at coexistence which yields $X_s^e = 1 - X_t^e \simeq 1$ and $X_t^c = 1 - X_t^c \lesssim 1$. It is noteworthy that, while at temperatures above $u/kT \cong 0.4$ the e$\rightarrow$c transition is indicated by a van der Waals-like loop in the π and μ

isotherms, below this temperature the system 'jumps' from one free energy branch to another.

A qualitative explanation of the decrease in ρ_c with T can be given as follows: As $\rho_e \to 0.25$ and $X_s \to 1$, the energy ε_e and the translational entropy s_e (per particle) of the (s-particle saturated) monolayer approach constant values, $\bar{\varepsilon}_e$ and $\bar{s}_e$. (In our model $\bar{\varepsilon}_e = \frac{1}{2}4u_{ss} = -4u$ and $\bar{s}_e = 0$). Using ε_c and s_c to denote the corresponding quantities for the c phase, the temperature of the coexisting phases is given by

$$T = [\Delta\varepsilon + \pi\,\Delta(1/\rho)]/(\Delta s - k \ln \kappa)\,, \tag{21}$$

with $\Delta\varepsilon = \varepsilon_c - \varepsilon_e = \varepsilon_c - \bar{\varepsilon}_e$, $\Delta s = s_c - s_e = s_c - \bar{s}_e$, and $\Delta(1/\rho) = 1/\rho_c - 1/\rho_e = 1/\rho_c - 4$.

The term $k \ln \kappa$ in the denominator accounts for the difference in internal free energy per particle in the coexisting phases $\Delta f_{int}/T = -\Delta s_{int} = k \ln \kappa$ which, in the present analysis, is independent of T. (In addition we assume, as confirmed by the calculations, that $X_t^c \simeq 1$). The energy of the e phase is given (in the mean-field approximation) by $\varepsilon_c \simeq \frac{1}{2}\rho_c 4u_{tt} = -8\rho_c u$, thus $\Delta\varepsilon \simeq -4u(2\rho_c - 1)$. The translational entropy is $s_c/k \cong \ln[(1-\rho_c)/\rho_c] - (1/\rho_c) \times \ln(1-\rho_c)$. For $\kappa = 100$ and, say, $\rho_c > 0.5$, we find $|\Delta s| = s_c \ll k \ln \kappa$. Thus, the denominator in (21) decreases (slowly, in absolute value) with ρ_c. On the other hand, the numerator decreases nearly linearly (in absolute value) since $\Delta\varepsilon + \pi\,\Delta(1/\rho) \sim 4u(2\rho_c - 1) - \pi(4 - 1/\rho_c)$. This explains, qualitatively, why ρ_c decreases with T. In this connection it should be mentioned that a decrease in the density of the liquid-condensed phase upon cooling, has in fact been observed in a number of experimental monolayer studies [2,6,7].

When T falls below a critical temperature T_c^{ge}, corresponding to $u/kT_c^{ge} \simeq 0.5$, the monolayer undergoes another, gas–liquid, transition which is completed at densities $\rho < 0.25$. Since for large κ, at this density range, the monolayer consists almost exclusively of s-particles, this transition is a simple condensation of s-particles. The critical value $u_{ss}/kT_c^{gl} = -2u/kT_c^{gl} = -1$ is, indeed, the common (Bragg–Williams) [21] value for a lattice gas of particles interacting through nearest-neighbor attractions u_{ss} on a square lattice. Thus, there is a range of temperatures, over which the system exhibits, upon compression, two successive first order transitions. For large κ, the first gas–liquid transition is a simple condensation of the s-particles (which are reluctant to yield their high free energy content), while the second involves a large change in the monolayer's composition.

In fig. 2, and more clearly in fig. 3, which shows $\mu - \rho$ isotherms, we see that at still lower temperatures the monolayer goes directly from the gas phase (of s-particles) to a condensed phase (consisting mostly of t-particles). This g–c

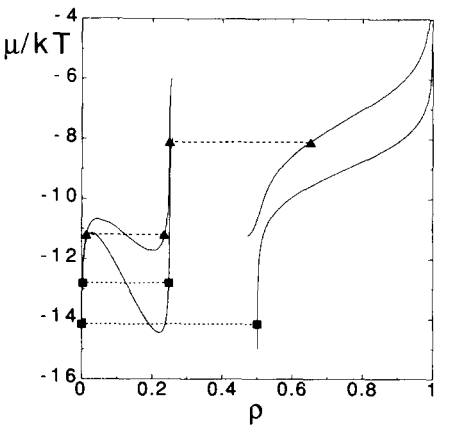

Fig. 3. Chemical potential (μ)–density (ρ) isotherms for $\kappa = 100$ at $u = 0.8$ (triangles) and $1.2kT$ (squares). Note that for $u = 0.8$ $\mu_{cc} > \mu_{ge}$ while for $u = 1.2$ the inequality is reversed, indicating that the g–c transition preempts the g–e transition.

transition preempts the gas–liquid transition. In other words, the monolayer has a triple point ($u/kT_{tp} \simeq 1.0$ for $\kappa = 100$), below which the intermediate phase of densely packed s-particles becomes metastable. The existence of a triple point in surfactant monolayer systems has been observed in many experiments [6].

Monte Carlo simulations for the monolayer of interconverting squares ($s \rightleftharpoons t$) support the qualitative conclusions derived from the mean-field analysis. *NMT* simulations were performed for a monolayer adsorbed on a 100×100 square lattice, with periodic boundary conditions. Fig. 4 shows two snapshots of a 50×50 section of the lattice, for a monolayer with $\kappa = 100$ and $u/kT = 1$. Fig. 4a describes a typical monolayer pattern at the g–e coexistence region, i.e., the average density ($\rho = 0.1$) is intermediate between the densities $\rho^g \simeq 0.05$, and $\rho^e \simeq 0.20$ of the coexisting phases. As expected for the large value of κ, as long as $\rho < 0.25$, the monolayer consists mostly of large squares (s-particles). We note the existence of (small) domains of the liquid phase, surrounded by a dilute gaseous phase. Calculations of the chemical potential (by the insertion method) [20] and the pressure confirm that the monolayer, of which a section is shown in fig. 4a, is indeed in the g–e coexistence region, see fig. 5.

Fig. 4b shows a typical monolayer section corresponding to the second 'chemical' (or e–c) transition. Dense domains of s-particles coexist with similarly dense domains of t-particles. As ρ increases, the number and size of the t-domains increase at the expense of the s-domains.

As κ decreases, X_s (at $\rho \to 0$) decreases as well, as a result of the low free energy content of the s-particles and hence their resistance to conversion into

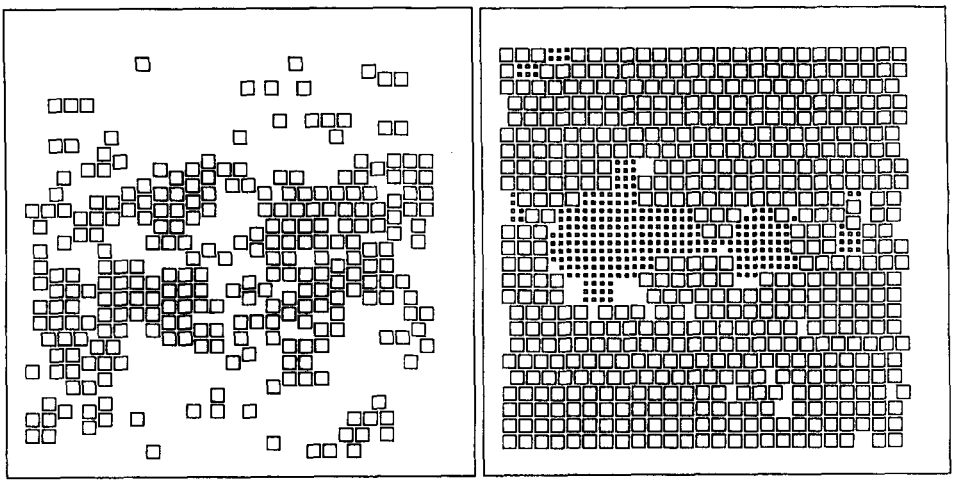

Fig. 4. Snapshots of typical configurations from Monte Carlo simulations of a monolayer with $\kappa = 100$ and $u = 1kT$ (shown are 50×50 sections from a 100×100 sites simulation). (a) corresponds to the g–e coexistence region, and (b) is a typical e–c configuration.

the t-form. Consequently, the intermediate e phase (with $\rho \simeq 0.25$, $X_s \simeq 1$) is expected to gradually lose its stability relative to the c phase in which the excluded area and the attractive inter-(t)-particle forces are more favorable. Indeed, from fig. 6, which shows $\pi-\rho$ isotherms for $\kappa = 4$, we see that the g–c transition preempts the g–e transition already for $u/kT \leqslant 0.6$, whereas for $\kappa = 100$ this only occurs at $u/kT \leqslant 1.2$. At any temperature, the range of stability of the e phase continues to narrow down and hence T_{tp} increases, as κ

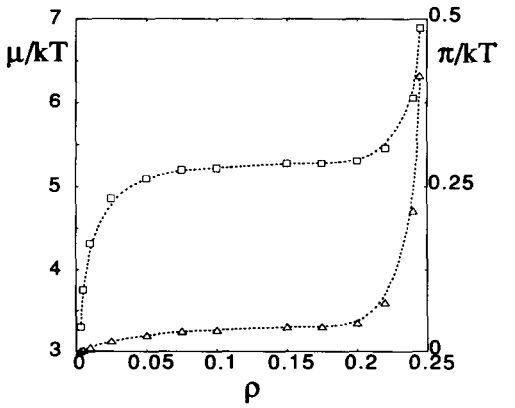

Fig. 5. Chemical potential (μ) (squares) and pressure (π) (triangles) vs. density (ρ) isotherms obtained from the Monte Carlo simulation for the same parameters as in fig. 4a (the g–e region).

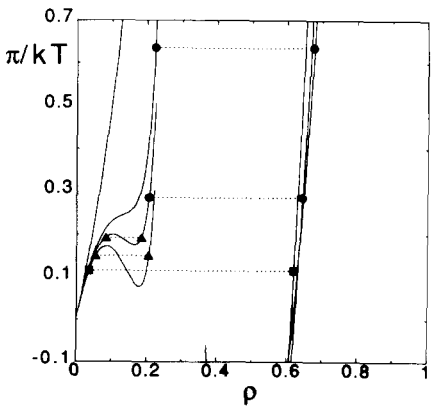

Fig. 6. Pressure (π)–density (ρ) isotherms from the mean field calculations for $\kappa = 4$ at $\mu = 0, 0.5, 0.55$ and $0.6kT$. The circles, triangles and squares correspond, respectively, to the g–e, e–c and g–c transitions.

decreases. This conclusion is consistent with experimental findings which show that in amphiphilic monolayers T_{tp} decreases as the chain length of the adsorbed molecule increases [2]. (Recall that large κ corresponds to large free energy content of the molecules in the expanded state, which increases with chain length).

At some point, as κ is lowered at constant u/kT, the intermediate e phase disappears completely, even as a metastable phase. This is illustrated in fig. 7 which shows the mean-field calculations for $u/kT = 0.6$ for $\kappa = 2.5$ and 2. For $\kappa = 2.5$, the g–c transition preempts the g–e transition, as the system jumps from the g to the c branch, but the e phase is reminiscent through the g–e loop. For $\kappa = 2$ there is only one loop connecting the g and c phases with no signature of the e phase.

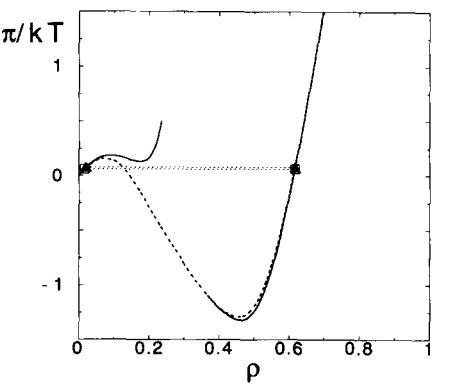

Fig. 7. Pressure (π)–density (ρ) isotherms from the mean-field calculations for $u = 0.6kT$ and $\kappa = 2$ (dashed line) and 2.5 (solid line).

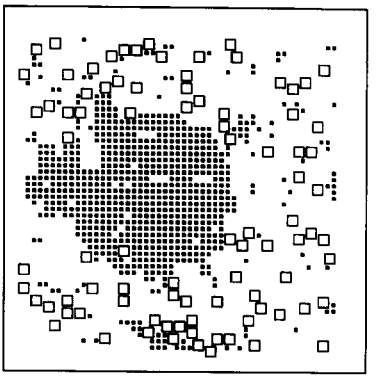

Fig. 8. A typical configuration from Monte Carlo simulation for $\kappa = 2$ at $u = 0.5\,kT$, illustrating the phase coexistence in the g–c transition region. (The figure shows a 50×50 section from a simulation of a 100×100 lattice.)

Finally, we note that the g–c transition involves large changes in both the density and the composition of the monolayer. Thus, the 'chemical' and 'gas–liquid' aspects of the g–c transition are strongly mixed, or, in other words, both ρ and X_t/X_s are relevant (coupled) order parameters. Our MC simulations support the conclusion that at low T or low κ the system goes directly from the g to the c phase. This is clearly illustrated in fig. 8 which shows domains of the two coexisting phases.

The absence of an intermediate phase (the e phase in our model) in a monolayer comprised of molecules with low free energy content (low κ) is consistent with recent experimental measurements [5]. In these experiments it was found that the le phase does not appear in a monolayer of stiff (perfluorinated) molecules, whose conformational free energy is negligible. The le phase re-appears upon replacement of some of the CF_2 segments by CH_2 groups which leads to higher chain flexibility.

5. Concluding remarks

Our goal in this paper has been to demonstrate that some of the more important characteristics of surfactant monolayers can be cast in simple thermodynamic terms using a highly simplified 'molecular' model. Our mean-field analysis and MC simulations have shown, for example, that a high free energy content of the unperturbed molecules is a necessary condition for the existence of a stable intermediate ('liquid expanded') phase, and, hence, for the possible observation of two successive phase transitions. The model, despite (or, perhaps, because of) its simplicity could also explain more subtle

features of the monolayer phase diagram, such as the decrease of the triple-point temperature with increasing chain length, or the gradual decrease with temperature of the density of the liquid condensed phase.

Acknowledgements

We would like to thank Prof. William Gelbart for many helpful discussions and suggestions. We thank the Yeshaya Horowitz Association for financial support. The Fritz Haber Research Center is supported by the minerva Gesellschaft für die Forschung, mbH, Munich, BRD.

References

[1] G.L. Gaines, Insoluble Monolayers at Liquid Gas Interface (Wiley, New York, 1966).
[2] C.M. Knobler, Adv. Chem. Phys. 77 (1990) 397.
[3] (a) A.M. Bibo, C.M. Knobler and I.R. Peterson, J. Phys. Chem. 95 (1991) 5591.
(b) A.M. Somoza and R.M. Desai, J. Phys. Chem. 96 (1992) 1401.
(c) S. Grayer-Wolf, M. Deutch, E.M. Lahav, L. Leiserowitz, K. Kjaer and J. Als-Nielsen, Science 242 (1988) 1286.
(d) J. Daillant, L. Bosio, B. Harzallah and J.J. Benattar, J. Phys. (Paris) II 1 (1991) 149.
(e) K. Kjaer, J. Als-Nielsen, C.A. Helm, P. Tippman-Krayer and H. Möhwald, J. Phys. Chem. 93 (1989) 3200.
(f) S. Shin and S.A. Rice, J. Chem. Phys. 92 (1990) 1495.
(g) G. Cardini, J.P. Bareman and M.L. Klein, Chem. Phys. Lett. 145 (1988) 493.
(h) H.M. McConnell, Ann. Rev. Phys. Chem. 42 (1991) 171.
[4] (a) N.R. Pallas and B.A. Pethica, J. Chem. Soc. Faraday Trans. I 83 (1987) 585.
(b) N.R. Pallas and B.A. Pethica, Langmuir 1 (1985) 509.
[5] S.W. Barton, A. Goudot, O. Bouloussa, F. Rondelez, B. Lin, F. Novak, A. Acero and S.A. Rice, J. Chem. Phys. 96 (1992) 1343.
[6] B.C. Moore, C.M. Knobler, S. Akamatsu and F. Rondelez, J. Phys. Chem. 94 (1990) 4588.
[7] J. Daillant, L. Bosio and J.J. Benattar, Europhys. Lett. 12 (1990) 715.
[8] (a) R.S. Cantor and P.M. McIlroy, J. Chem. Phys. 90 (1989) 4423; (b) 4431; (c) 91 (1989) 416.
[9] S. Shin, Z-G. Wang and S.A. Rice, J. Chem. Phys. 92 (1990) 1427.
[10] C.M. Roland, M.J. Zuckermann and A. Georgallas, J. Chem. Phys. 86 (1987) 5852.
[11] D. Kramer, A. Ben-Shaul, Z-Y. Chem and W.M. Gelbart, J. Chem. Phys. 96 (1992) 2236.
[12] Z-Y. Chen, J. Talbot, W.M. Gelbart and A. Ben-Shaul, Phys. Rev. Lett. 61 (1988) 1376.
[13] J. Harris and S.A. Rice, J. Chem. Phys. 88 (1987) 1298.
[14] I. Szleifer, A. Ben-Shaul and W.M. Gelbart, J. Chem. Phys. 94 (1990) 5081.
[15] Z-G. Wang, J. Phys. (Paris) 51 (1990) 1431.
[16] L. Onsager, Ann. N.Y. Acad. Sci. 51 (1949) 627.
[17] R.W. Zwanzig, J. Chem. Phys. 39 (1963) 1714.
[18] D.P. Fraser, M.J. Zuckermann and O.G. Mouritsen, Phys. Rev. A 43 (1991) 6642.
[19] N. Metropolis, A.W. Rosenbluth, M.N. Rosenbluth, A.N. Teller and E. Teller, J. Chem. Phys. 21 (1953) 1087.
[20] B. Widom, J. Chem. Phys. 39 (1963) 2808.
[21] T.L. Hill, Statistical Mechanics (McGraw-Hill, New York, 1956).